Steady Symmetric Flow Past Elliptical Cylinders

Jacob H. Masliyah and Norman Epstein

Chemical Engineering Department, University of British Columbia, Vancouver, B. C., Canada

Numerical methods have been used to investigate the steady incompressible flow past symmetrically oriented elliptical cylinders for Reynolds numbers up to 90. The ratio of minor to major axis of the cylinders studied ranged from 0.2 to 1.0. The surface pressure distribution and the skin and form drag coefficients were numerically evaluated for the various Reynolds numbers. The results for frontal stagnation pressure and boundary layer thickness are in good agreement with boundary layer theory. The wake size was found to be a strong function of the cylinder shape, orientation, and Reynolds number. Streamlines, iso-vorticity lines, and equi-velocity lines are presented and show in detail the flow characteristics.

Flow past elliptical cylinders arises in certain heat exchangers (Knudsen and Katz, 1958) as well as in some textile fibres. The steady motion of a viscous incompressible Newtonian fluid past an immersed body is governed by the Navier–Stokes equation, subject to the prevailing boundary conditions. Due to its nonlinearity, this equation has so far proved insoluble for the problem of flow past an elliptical cylinder (a circular cylinder and a plate being the limiting forms), except by techniques which linearize approximately the equations of motion. A complete neglect of the nonlinear terms of the Navier–Stokes equation led to "Stokes' Paradox" where no physically meaningful solution could be obtained (Krakowski and Charnes, 1953; Stokes, 1851). Lamb (1932) successfully applied Oseen's (1927) equations to the case of flow past a circular cylinder. Lamb's solution has been improved by Tomotika and Aoi (1950, 1951). Kaplun (1957) applied the method of inner and outer expansions to obtain the drag force experienced by the cylinder.

Oseen's equations were solved approximately for the case of elliptical cylinders by Bairstow, *et al.* (1923), and Harrison (1924), and more rigorously by Tomotika and Aoi (1953) and Imai (1954). These solutions are limited by the nature of the Oseen approximation and prove to be inadequate above Reynolds number 2.

A finite difference method was used by Thom (1929, 1931, 1933) to solve the Navier–Stokes equation for flow past circular cylinders at $Re = 10$ and 20, and the same method has been used by Kawaguti (1953) for $Re = 40$. This method, which is very tedious, was converted into a relaxation scheme by Fox (1944, 1947, 1948), Southwell, *et al.* (1945), and Allen and Dennis (1951). Hamielec and Raal (1969) obtained solutions up to $Re = 500$ but, as indicated by Dennis and Chang (1969), their results do not represent a truly isolated cylinder for $Re > 50$. Several other workers have obtained results on unsteady flow past a circular cylinder, in some cases carrying the transient calculations to sufficiently long times that the attainment of steady state could be safely assumed (Son and Hanratty, 1969; Thoman and Szewczyk, 1969).

Dennis and Chang (1969) have recently presented results for flow at $Re = 0.2$–40 along the major axis of an elliptical cylinder, the ratio of minor to major axis of which was 0.2. Their method consisted of numerically integrating the time-dependent equations of motion to a large enough time for "steady state" to have been reached.

Governing Equations

The Navier–Stokes equation for steady flow past an elliptical cylinder, in terms of the stream function (Goldstein, 1938), is

$$\nu E'^4\psi' = \frac{1}{c^2(\sinh^2\xi + \sin^2\eta)}\left\{\frac{\partial(\psi', E'^2\psi')}{\partial(\xi,\eta)}\right\} \tag{1}$$

where

$$E'^2 = \frac{1}{c^2(\sinh^2\xi + \sin^2\eta)}\left\{\frac{\partial^2}{\partial\xi^2} + \frac{\partial^2}{\partial\eta^2}\right\} \tag{2}$$

Equations 1 and 2 are in elliptical cylindrical coordinates (Happel and Brenner, 1965) and assume that the undisturbed flow is parallel to the major axis. The minor semi-axis, b, is given by $b = c\sinh\xi_a$.

The following dimensionless quantities are now defined.

$$\psi = \psi'/Ub; \quad E^2 = c^2E'^2; \quad Re = 2bU/\nu$$

The two-dimensional symmetric flow is then governed by

$$\frac{2}{Re}E^4\psi = \frac{1}{\sinh^2\xi + \sin^2\eta}\left\{\frac{\partial\psi}{\partial\xi}\frac{\partial E^2\psi}{\partial\eta} - \frac{\partial\psi}{\partial\eta}\frac{\partial E^2\psi}{\partial\xi}\right\} \tag{3}$$

and

$$E^2 = \frac{1}{\sinh^2\xi + \sin^2\eta}\left\{\frac{\partial^2}{\partial\xi^2} + \frac{\partial^2}{\partial\eta^2}\right\} \tag{4}$$

instead of Equations 1 and 2, respectively. Equation 3 can be split into two parts, after Thom (1929), one in terms of ψ, ξ, and η and the other in terms of ζ, ξ, and η, to give

$$E^2\zeta = \frac{Re}{2}\frac{1}{\sinh^2\xi + \sin^2\eta}\left\{\frac{\partial\psi}{\partial\xi}\frac{\partial\zeta}{\partial\eta} - \frac{\partial\psi}{\partial\eta}\frac{\partial\zeta}{\partial\xi}\right\} \tag{5}$$

and

$$E^2\psi = \zeta/\sinh^2\xi_a \tag{6}$$

where ζ is the dimensionless vorticity defined as $\zeta = \zeta' b/U$, the dimensional vorticity being

$$\zeta' = E'^2\psi' \tag{7}$$

The computational field is confined between an inner surface (the elliptical cylinder) and an outer envelope, which

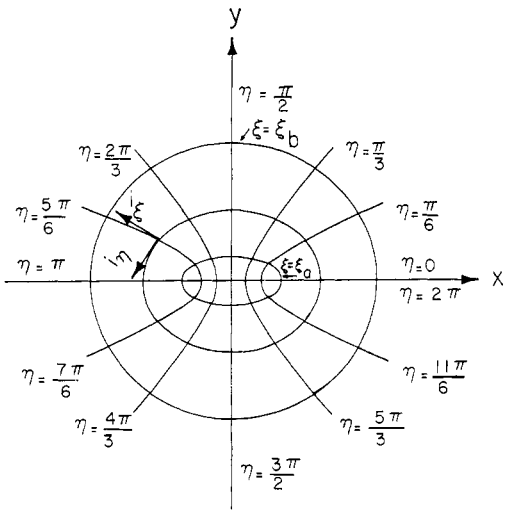

Figure 1. Elliptical cylinder coordinates

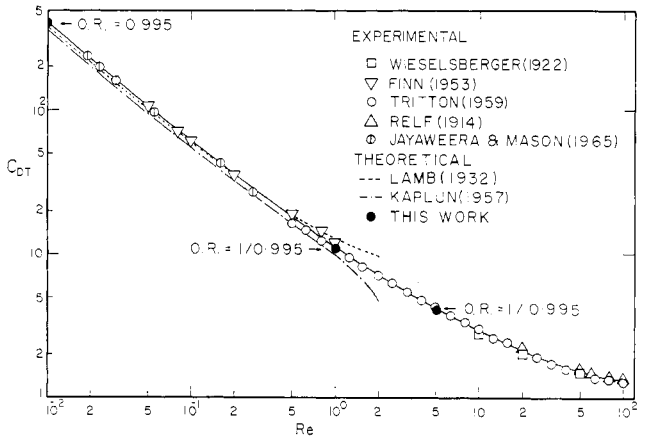

Figure 2. Drag coefficients for circular cylinders

is made to conform with an elliptical coordinate grid line (see Figure 1).

The four boundary conditions defining the flow are given by specifying two boundary conditions each for the stream function and the vorticity. At the surface of the cylinder the no-slip condition leads to $\psi = 0$ and

$$\zeta_{\xi=\xi_a} = \frac{\sinh^2 \xi_a}{\sinh^2 \xi_a + \sin^2 \eta} \frac{\partial^2 \psi}{\partial \xi^2}\bigg|_{\xi=\xi_a}$$

At the outer envelope the flow is assumed to be in streaming parallel flow, whereby

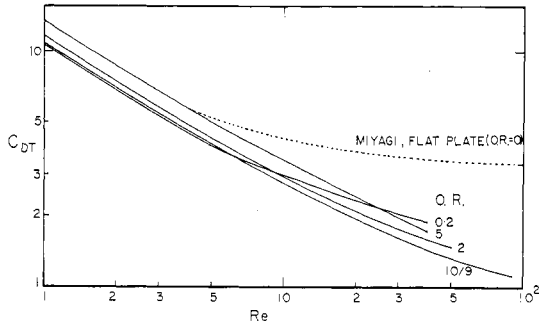

Figure 3. Variation of total drag coefficient with Reynolds number for elliptical cylinders

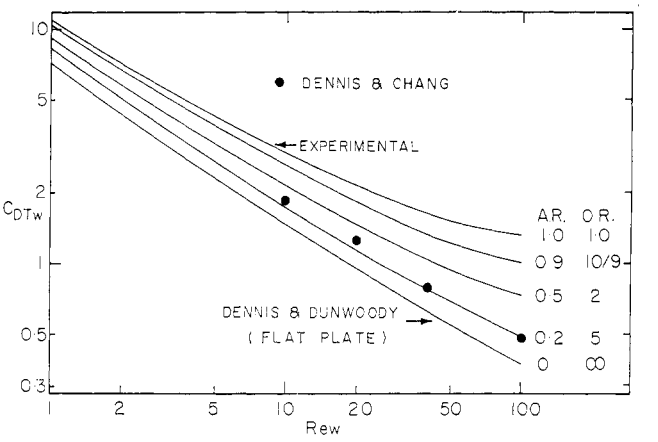

Figure 4. Variation of total drag coefficient with Reynolds number for flow along the major axis, which is taken as the characteristic length

$$\psi = \sin \eta \sinh \xi_b \operatorname{cosech} \xi_a$$

and $\zeta = 0$. Along the axis of symmetry ($\eta = 0, \pi$) both ψ and ζ are zero.

The drag on a body is usually expressed in terms of a dimensionless drag coefficient

$$C_D = \frac{\text{drag force in the flow direction}}{\left(\begin{matrix}\text{projected area normal to} \\ \text{the direction of flow}\end{matrix}\right) \times {}^1/_2\rho U^2}$$

It is relatively easy to show that the skin (surface) drag coefficient, C_{DS}, is given by

$$C_{DS} = \frac{4}{Re} \coth \xi_a \int_0^\pi \zeta_{\xi=\xi_a} \sin \eta \, d\eta \qquad (8)$$

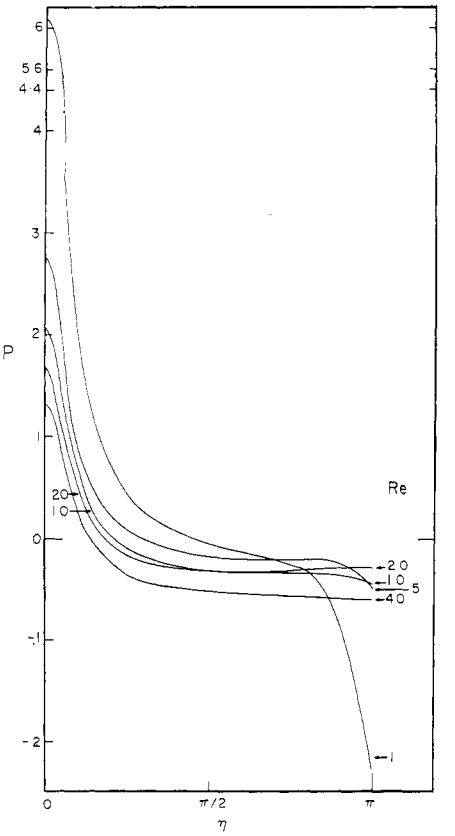

Figure 5. Surface pressure distribution for an elliptical cylinder with O.R. = 5

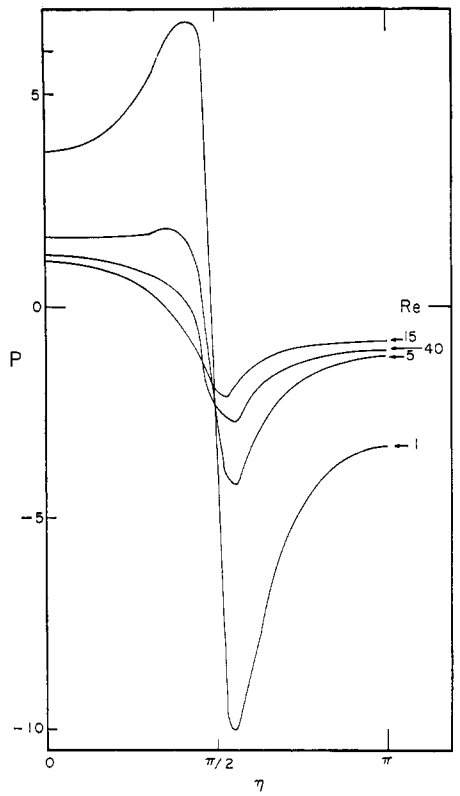

Figure 6. Surface pressure distribution for an elliptical cylinder with O.R. = 0.2

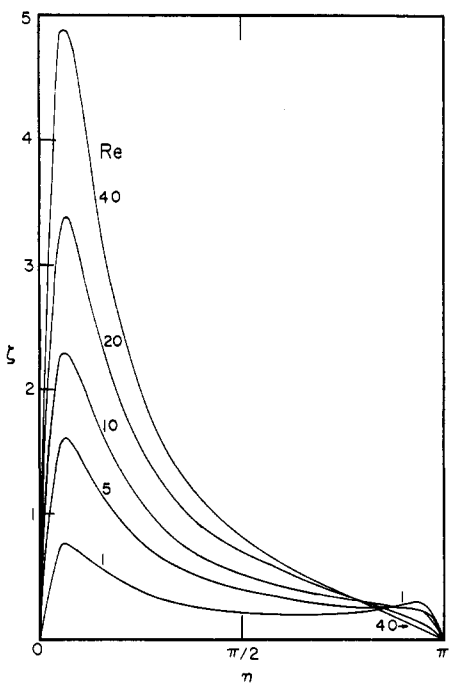

Figure 7. Surface vorticity distribution for an elliptical cylinder with O.R. = 5

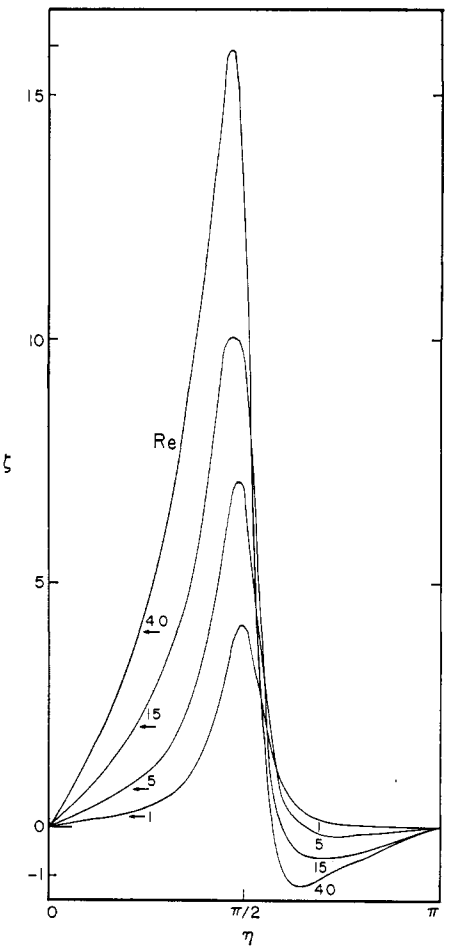

Figure 8. Surface vorticity distribution for an elliptical cylinder with O.R. = 0.2

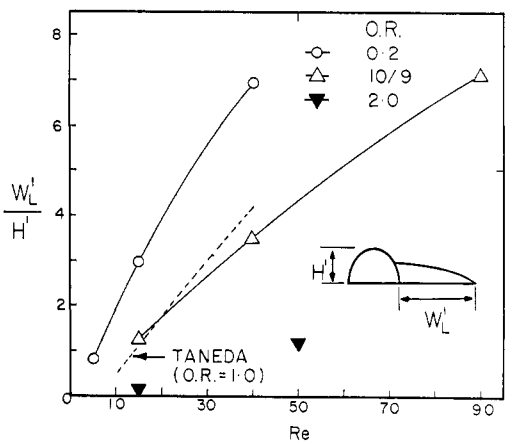

Figure 9. Variation of wake length with Re for elliptical cylinders

The dimensionless surface pressure, P, can be deduced, from a consideration of the η component of the Navier–Stokes equation, as

$$P - P_o = \frac{4}{Re}\int_0^{\eta} \left.\frac{\partial \zeta}{\partial \xi}\right|_{\xi=\xi_a} d\eta \qquad (9)$$

The frontal stagnation pressure, P_o, is obtained from a consideration of the ξ component of the Navier–Stokes equation, which gives

$$P_o = 1 + \frac{4}{Re}\int_{\xi_a}^{\xi_b} \left.\frac{\partial \zeta}{\partial \eta}\right|_{\eta=0} d\xi \qquad (10)$$

The form (pressure) drag coefficient is

$$C_{DF} = \int_0^{\pi} P \cos\eta \, d\eta \qquad (11)$$

The total drag is then obtained by adding C_{DS} and C_{DF}.

Table I. Grid Size and Drag Coefficients for Elliptical Cylinders

O.R.	Re	d_m	A	B	C_{DS}	C_{DF}	C_{DT}
0.2	1.0	133	0.05	0.0982	1.7795	9.0302	10.810
0.2	5.0	133	0.05	0.0982	0.6096	3.3326	3.942
0.2	15	133	0.05	0.0982	0.3097	2.2763	2.586
0.2	40	133	0.0442	0.0491	0.1725	1.6419	1.814
0.995	0.01	8102	0.0865	0.0785	199.2	201.5	400.7
1/0.995	1.0	257	0.0603	0.0982	5.3144	5.4645	10.779
1/0.995	5.0	121	0.0522	0.0982	1.8911	2.1606	4.052
10/9	1.0	134	0.0532	0.0982	5.6834	5.227	10.911
10/9	5.0	134	0.0532	0.0982	1.9653	2.0811	4.046
10/9	15	134	0.0532	0.0982	1.0014	1.2454	2.2468
10/9	40	134	0.0471	0.0491	0.5587	0.8613	1.420
10/9	90	134	0.0471	0.0491	0.3156	0.8017	1.117
2	0.5	111	0.0506	0.0982	12.544	6.2752	18.820
2	1.0	111	0.0506	0.0982	7.6772	4.0149	11.692
2	5.0	111	0.0506	0.0982	2.6885	1.6093	4.298
2	15	111	0.0506	0.0982	1.4142	0.9648	2.379
2	50	111	0.0506	0.0982	0.7163	0.7524	1.469
5	1.0	60	0.0558	0.0982	11.577	2.4375	14.014
5	1.0	133	0.050	0.0982	11.236	2.3700	13.607
5	5.0	133	0.050	0.0982	4.0465	0.9721	5.019
5	10	133	0.050	0.0982	2.7229	0.7665	3.490
5	20	133	0.050	0.0982	1.8338	0.5899	2.424
5	40	133	0.050	0.0982	1.1146	0.6559	1.771

The corresponding equations for the case of symmetric flow along the minor axis of the elliptical cylinder can be obtained simply by replacing each c with $-ic$, sinh ξ with i cosh ξ, and cosh ξ with i sinh ξ. Using this procedure the term b now represents the major semi-axis, but the Reynolds number, Re, is again based on the axis, $2b$, perpendicular to the flow direction.

Numerical Analysis Procedure

Equations 5 and 6 were expressed in finite difference form using a Taylor expansion to the second order and were solved simultaneously using a relaxation procedure. Relaxation factors were introduced by which the change in the estimated values of ψ and ζ between successive iterations was magnified for ψ and reduced for ζ. This was helpful in obtaining relatively fast convergence and stable values of flow functions at the lattice points. Details of the relaxation scheme are given by Masliyah (1970) and Masliyah and Epstein (1970).

Convergence of the computed values for the stream function and vorticity was assumed when no further change was apparent in the fourth significant figure of any function between successive iterations. With such a tolerance the drag coefficients and surface pressure distributions would not change by more than 0.5% and 1.0%, respectively, for a further 50 iterations. For very low Re (Re = 0.01) the convergence criterion was taken as no further change in the fifth significant figure. The spacing in both the ξ and η directions for the cases considered are given in Table I. As the position of the outer envelope is important, the minimum mean diameter was taken as 111, which is far enough to have negligible influence on the flow pattern near the surface of the elliptical cylinders.

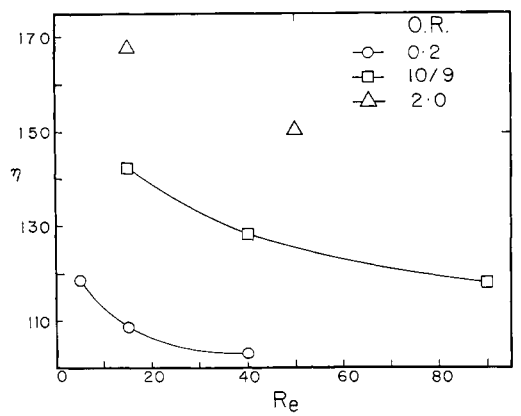

Figure 10. Location of separation point for elliptical cylinders

Numerical Results

The numerical work on circular cylinders has been well covered by previous workers. Initial work on a nearly circular elliptical cylinder was done to test the computer program. A ratio of minor to major axis of 0.995 was used to represent a circle in elliptical coordinates. Figure 2 shows the experimental data on drag coefficients of various workers, together with the analytical solutions of Lamb (1932) and Kaplun (1957), as well as the present numerical work. The numerical results at Re = 0.01 for O.R. = 0.995 and at Re = 1 and 5 for O.R. = 1/0.995 agree very well with the experimental data of the various workers. It is interesting that Lamb's solution is quite accurate in estimating the total drag coefficient up to Re = 1.0. The experimental work of Jayaweera and Mason (1965) at $Re \simeq 0.02$ shows that Lamb's solution still holds at this very low Reynolds number. It should be borne in mind that there is no valid creeping flow solution for

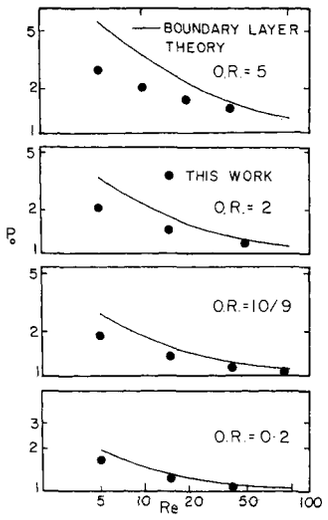

Figure 11. Variation of the frontal stagnation pressure with Reynolds number for elliptical cylinders

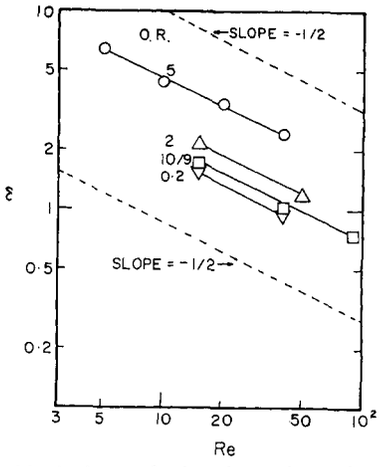

Figure 12. Variation of the boundary layer thickness with Reynolds number for elliptical cylinder at $\eta = \pi/2$

the circular cylinder, since Stokes' solution gives zero drag coefficient when the outer envelope is at infinity (Happel and Brenner, 1965). At $Re = 0.01$ the presence of the outer boundary is very influential in determining the exact value of the total drag coefficient. For $d_m = 257$, it was found that C_{DT} obtained by the numerical solution of the complete Navier–Stokes equation agrees with that obtained by the analytical creeping flow solution of Kuwabara (1959). However, this value of C_{DT} is about 30% higher than the experimental value. For $d_m = 8102$, the numerically computed value of C_{DT} is very close to the experimental data, indicating that the influence of the outer envelope is negligible, but the creeping flow solution then gives a value that is 20% lower than the experimental data.

The total drag coefficient, based on that axis of the elliptical cylinder which is perpendicular to the flow direction, is plotted in Figure 3, where it is seen that C_{DT} does not vary much with O.R. over the range computed. It is interesting that at $Re < 6$, flow along the minor axis of an elliptical cylinder with O.R. = 0.2 shows values of C_{DT} lower than those obtained for flow along the major axis (O.R. > 1). However, for higher Re, the curve of C_{DT} *vs.* Re for O.R. = 0.2 crosses and exceeds all the others. The work of Miyagi (1968) for flow perpendicular to flat plates (O.R. = 0) gives values of C_{DT} much higher than those computed for O.R. = 0.2 at higher Re. The reason for the slower rate of decrease in C_{DT} with Re for the lower orientation ratios is probably the early formation of a wake bubble, which gives rise to additional form drag.

In order to compare the total drag coefficient with that of a flat plate set parallel to the main direction of the flow, C_{DTw} is plotted against Rew in Figure 4, the subscript w signifying that the coordinates are both based on the width of the elliptical cylinder, *i.e.*, on the axis along the flow direction. It is seen that the results for O.R. = 5, 2, and $^{10}/_{9}$ between those for a circular cylinder (O.R. = 1.0) and those for a flat plate (O.R. = ∞), as computed numerically by Dennis and Dunwoody (1966). The results of Dennis and Chang for O.R. = 5 are plotted for comparison. Good agreement was obtained for $Rew = 100$ and 40. However, at $Rew = 20$ and 10 their values fell higher than those given by this work. This could be due to the coarse grid size used by them at the lower Reynolds numbers. Their values of $A(= B)$ for $Rew =$ 10, 20, 40, and 100 were 0.157, 0.157, 0.104, and 0.0785, respectively. The considerably lower values of A and B used in the present work, together with the computed values of the drag coefficients, are listed in Table I.

The dimensionless pressure distribution at the surface of the elliptical cylinders for various Reynolds numbers is given in Figures 5 and 6. At O.R. = 5 (Figure 5) a flat pressure distribution was obtained on the elliptical cylinder, except for the leading and trailing edges at low Re and the leading edge at higher Re. At O.R. = 0.2 (Figure 6) a maximum was observed for P at low Re, similar to that found by Masliyah (1970) in the case of an oblate spheroid with A.R. = 0.2. Such a maximum did not, however, appear for Re higher than about 5.

The surface vorticity is directly related to the shear stress at the cylindrical surface. Figures 7 and 8 show the surface

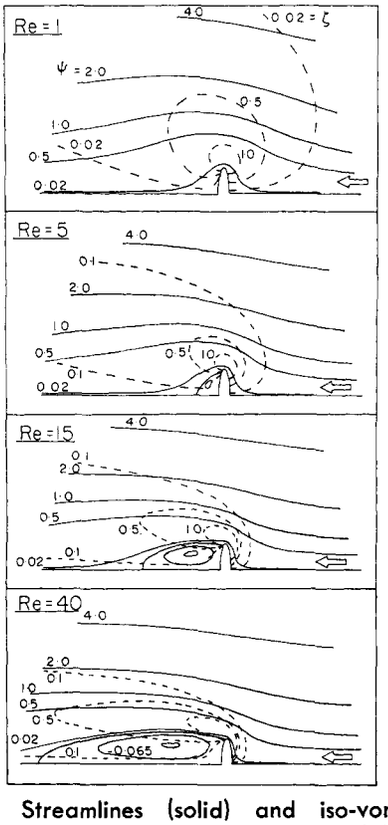

Figure 13. Streamlines (solid) and iso-vorticity lines (dashed) for an elliptical cylinder with O.R. = 0.2

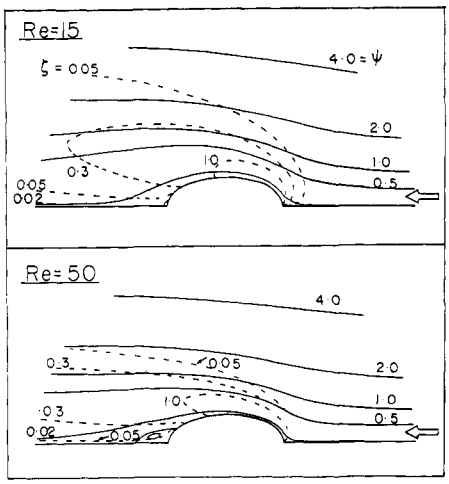

Figure 14. Streamlines (solid) and iso-vorticity lines (dashed) for an elliptical cylinder with O.R. = 2

vorticity distribution for different Reynolds numbers. At O.R. = 5 (Figure 7), there exist two maxima for $Re = 1.0$. The maximum nearer the trailing edge disappears for $Re > 5$ and the main contribution to the skin drag is then from the leading edge of the elliptical cylinder. At O.R. = 0.2 (Figure 8), the surface vorticity exhibits one maximum near the midzone of the cylinder and, beyond $\eta = \pi/2$, it changes sign very rapidly for the higher Re, indicating a reversal in the flow direction and hence separation.

The variation of the dimensionless wake length with Re for the elliptical cylinders is shown in Figure 9. For O.R. = 0.2, at $Re = 40$, the wake length is already several times the length of the major axis. Such long two-dimensional wakes are in general not stable, and shedding usually occurs (Marris, 1964). The experimental data of Taneda (1956) on circular cylinders are plotted for comparison. Figure 10 shows the angle of separation for O.R. = 0.2, $^{10}/_{9}$, and 2. For a nearly circular cylinder (O.R. $\simeq$ 1.0) at $Re = 5$, no separation was observed, and for O.R. = 5, no flow reversal was noted at Re as high as 40. For a circular cylinder, Dennis and Chang (1969) indicated a wake appearance at $Re \simeq 6.2$.

The variation of the dimensionless pressure with Re for the frontal stagnation point is compared with the first approximation (Homann, 1936) of boundary layer theory, in which the outside flow is taken to be a potential flow, in Figure 11. The agreement is very good for the higher Reynolds numbers, especially for O.R. < 0.2, as would be expected. The boundary layer thickness at $\eta = \pi/2$ for the various elliptical cylinders is shown in Figure 12. The edge of the boundary layer is taken at $|\partial v_\eta/\partial \xi| = 0$. From these plots it is seen that the boundary layer thickness varies as $Re^{-1/2}$, as predicted by boundary layer theory. Separation for the cases considered occurs beyond $\eta = \pi/2$.

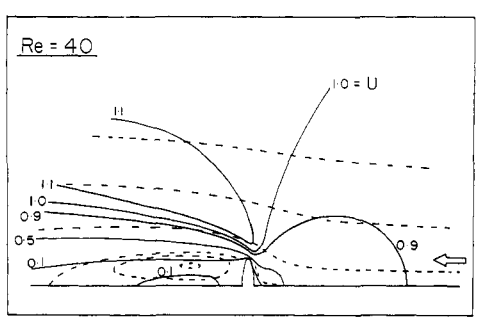

Fig. 15. Iso-velocity lines (solid) and streamlines (dashed) for an elliptical cylinder with O.R. = 0.2

The contouring of the streamlines and iso-vorticity lines for O.R. = 0.2 and 2 is shown in Figures 13 and 14. It has been reported by Van Dyke (1964) that the disturbance due to a two-dimensional object is in general more intense than that for a three-dimensional one. This is confirmed in the present work, in that at a given distance from the elliptical cylinder a given streamline is more curved than that found by the same authors (1970) for the corresponding spheroid (same A.R.; also O.R. < 1 for elliptical cylinder corresponds to oblate spheroid and O.R. > 1 to prolate spheroid). This result also indicates that the effect of a confining wall would be more appreciable for the cylinders than for the corresponding spheroids.

The deviation of the flow from the Stokes régime, in which symmetry prevails, is best illustrated by the dissymmetry of the iso-vorticity lines. The vorticity is generated upstream and is carried by the fluid to considerable distances downstream. These distances are a strong function of Reynolds number, as shown in Figures 13 and 14.

The equi-velocity lines at $Re = 40$ for O.R. = 0.2 are shown in Figure 15. The modulus of the velocity vector was found by using the Lagrange three-point formula on the stream function. The velocity contour clearly indicates that the velocity inside the wake is very small.

Acknowledgment

The authors are indebted to the University of British Columbia and to the National Research Council of Canada for continuing financial support.

Nomenclature

A = dimensionless increment in the ξ direction
A.R. = aspect ratio = ratio of minor to major axis
b = length of semi-axis normal to the net flow direction
B = dimensionless increment in the η direction
c = focal length of the elliptical coordinate system
C_{DF} = form drag coefficient
C_{DS} = skin drag coefficient
C_{DT} = total drag coefficient
C_{DTw} = total drag coefficient based on the axis of the elliptical cylinder parallel to the flow direction
d_m = mean diameter = total cross-sectional area of the outer envelope divided by the cross-sectional area of the cylinder, all raised to the power $^1/_2$
i = $\sqrt{-1}$
i_η = unit vector in the η direction
i_ξ = unit vector in the ξ direction
O.R. = orientation ratio = ratio of the axis parallel to the net flow direction to that perpendicular to the flow
P = dimensionless pressure, $P = (P' - P'_{ref})/(^1/_2 U^2 \rho)$
P' = dimensional pressure
P_o = dimensionless frontal stagnation pressure
P'_{ref} = dimensional reference pressure = pressure at infinity
Re = Reynolds number based on the axis normal to the net flow direction = $2bU/\nu$
Rew = Reynolds number based on the axis parallel to the net flow direction = $2b(\text{O.R.})U/\nu$
U = velocity of the undisturbed stream
v_η = dimensionless velocity component in the η direction

Greek Letters

δ = boundary layer thickness/b, dimensionless
ζ = dimensionless vorticity
ζ' = dimensional vorticity
η, ξ = elliptical coordinates
ν = kinematic viscosity
ρ = density

ψ = dimensionless stream function
ψ' = dimensional stream function

SUBSCRIPTS

a = surface of elliptical cylinder
b = outer envelope

Literature Cited

Allen, D. N. de G., Dennis, S. C. R., *Quart. J. Mech.* **4** (2), 199 (1951).
Bairstow, L., Cave, B. M., Lang, E. D., *Phil. Trans. Roy. Soc.* **A223**, 383 (1923).
Dennis, S. C. R., Dunwoody, J., *J. Fluid Mech.* **24**, 577 (1966).
Dennis, S. C. R., Chang, G. Z., Mathematical Research Center, University of Wisconsin Technical Report No. 859 (1969).
Finn, R. K., *J. Appl. Phys.* **24**, 771 (1953).
Fox, L., *Quart. J. Appl. Math.* **2**, 251 (1944).
Fox, L., *Proc. Roy. Soc., Ser. A* **190**, 31 (1947).
Fox, L., *Quart. J. Mech.* **1**, 253 (1948).
Goldstein, S. "Modern Developments in Fluid Dynamics," Clarendon Press, Oxford, 1938.
Hamielec, A. E., Raal, J. D., *Phys. Fluids* **12**, 11 (1969).
Happel, J., Brenner, H., "Low Reynolds Number Hydrodynamics," Prentice Hall, Englewood Cliffs, N. J., 1965, pp 394, 495.
Harrison, W. J., *Camb. Trans.* **23**, 71 (1924).
Homann, F., 1936 Translation: National Advisory Committee for Aeronautics, Washington, D. C., Technical Memorandum No. 1334 (1952).
Imai, I., *Proc. Roy. Soc., Ser. A* **224**, 141 (1954).
Jayaweera, K. O. L. F., Mason, B. J., *J. Fluid Mech.* **22**, 709 (1965).
Kaplun, S., *J. Math. Mech.* **6**, 595 (1957).
Kawaguti, M., *J. Phys. Soc. Jap.* **8**, 747 (1953).
Knudsen, J. G., Katz, D. L., "Fluid Dynamics and Heat Transfer," McGraw-Hill, New York, N. Y., 1958, p 323.
Krakowski, M., Charnes, A., Carnegie Institute of Technology Department of Mathematics, Technical Report No. 37, 1953.
Kuwabara, S., *J. Phys. Soc. Jap.* **14**, 527 (1959).
Lamb, H., "Hydrodynamics," 6th ed, Cambridge University Press, Cambridge, 1932.
Marris, A. W., *J. Basic Eng., Trans. ASME* **86**, 185 (1964).
Masliyah, J. H., Ph.D. Thesis, University of British Columbia, Vancouver, Canada, 1970.
Masliyah, J. H., Epstein, N., *J. Fluid Mech.*, **44**, 493 (1970).
Miyagi, T., *J. Phys. Soc. Jap.* **24**, 204 (1968).
Oseen, C. W. "Hydrodynamik," Leipzig, 1927.
Relf, E. F., Tech. Rep. & Memo Adv. Comm. Aero. (A.R.C.), No. 102, 1914.
Son, J. S., Hanratty, T. J., *J. Fluid Mech.* **35**, 369 (1969).
Stokes, G. G., *Trans. Cambridge Phil. Soc.* **9**, 8 (1851).
Southwell, R. V., *et al.*, *Phil. Trans.* **A239**, 419 (1945).
Taneda, S., *J. Phys. Soc. Jap.* **11**, 302 (1956).
Thom, A., Aero. Res. Centre, R. & M. No. 1194 (1929).
Thom, A., *Proc. Roy. Soc., Ser. A* **131**, 30 (1931).
Thom, A., *Proc. Roy. Soc. Ser. A* **141**, 651 (1933).
Thoman, D. C., Szewczyk, A. A., *Phys. Fluids* **12**, (II), 76 (1969).
Tomotika, S., Aoi, I., *Quart. J. Mech. Appl. Math.* **3**, 140 (1950).
Tomotika, S., Aoi, I., *Quart. J. Mech. Appl. Math.* **4**, 401 (1951).
Tomotika, S., Aoi, I., *Quart. J. Mech. Appl. Math.* **6**, 290 (1953).
Tritton, D. J., *J. Fluid Mech.* **6**, 577 (1959).
Van Dyke, D., "Perturbation Methods in Fluid Mechanics," Academic Press, New York, N. Y., 1964.
Wieselsberger, C., *Phys. Z.* **22**, 321 (1922).

RECEIVED for review August 24, 1970
ACCEPTED February 26, 1971

EXPERIMENTAL TECHNIQUES

Determination of Pore-Size Distribution in Porous Materials. Test of a Proposed Method

Donald E. Felch and Frank O. Shuck

Institute of Atomic Research and Department of Chemical Engineering, Iowa State University, Ames, Iowa 50010

A proposed method for determining pore-size distribution in porous materials by the measurement of the effect of liquid flow through the material on the rate of diffusion of a solute through the pores was tested. The liquid diffusion process permitted measurement of a sufficiently large range of flow rates and concentration levels that distributions of pore sizes could be deduced. The tests were conducted on fritted glass disks of medium and coarse porosity. Comparison of size distributions for two medium porosity disks indicated that there were significant differences in the distribution of pore sizes for these similar materials.

THE FLOW of fluids through porous materials is of interest in applications occurring in a number of disciplines. Collins (1961) and Scheidegger (1957) give excellent general treatments of the subject. Attempts to better characterize flow through porous materials have led to the definition of a number of properties of such materials, *e.g.*, porosity, permeability, specific internal area, pore size, and pore-size distribution. The present study was concerned primarily with pore-size distribution since other properties of porous beds can be related to the pore-size distribution.

The measurement of pore-size distribution is complicated by the irregularity of pore shape in most porous materials. This difficulty may be overcome by the assumption that all pores have a common geometric shape such as a cylinder. Effective pore size distributions based on this assumption have been measured by techniques employing injection of mercury (Ritter and Drake, 1945; Washburn, 1921) and water (Childs and Collis-George, 1950), X-ray scattering (Ritter and Erich, 1948; Schull and Roess, 1947), and adsorption (Barrett, *et al.*, 1951; Haley, 1962). In all of these tech-